Lab on a Chip

EWOD (electrowetting on dielectric) digital microfluidics powered by finger actuation

Cheng Peng,[a] Zhongning Zhang,[a] Chang-Jin "CJ" Kim[a] and Y. Sungtaek Ju*[ab]

We report finger-actuated digital microfluidics (F-DMF) based on the manipulation of discrete droplets *via* the electrowetting on dielectric (EWOD) phenomenon. Instead of requiring an external power supply, our F-DMF uses piezoelectric elements to convert mechanical energy produced by human fingers to electric voltage pulses for droplet actuation. Voltage outputs of over 40 V are provided by single piezoelectric elements, which is necessary for oil-free EWOD devices with thin (typically <1 μm) dielectric layers. Higher actuation voltages can be provided using multiple piezoelectric elements connected in series when needed. Using this energy conversion scheme, we confirmed basic modes of EWOD droplet operation, such as droplet transport, splitting and merging. Using two piezoelectric elements in series, we also successfully demonstrated applications of F-DMF for glucose detection and immunoassay. Not requiring power sources, F-DMF offers intriguing paths for various portable and other microfluidic applications.

Introduction

Microfluidic devices are attractive for portable applications, including point-of-care (POC) diagnosis, bio-surveillance, environment sampling, and forensic science. They offer advantages of low sample volume requirements and high reaction rates for rapid analyses. However, most microfluidic systems require bulky pumping and control systems as well as electrical outlets to power them, limiting their field applications.[1]

Previous studies proposed different approaches to circumventing these challenges. Battery-powered microfluidic devices with integrated microvalves and micropumps, for example, have been reported for carrying out biological assays.[2] The resulting systems, however, were still too bulky for portable operations. "Passive" pumping mechanisms were also explored. Paper-based microfluidic devices based on capillary wicking attracted a lot of attention due to its perceived low cost, lightweight and disposability.[3,4] Other passive pumping mechanisms investigated include osmotic pressure,[5] built-in vacuum[6] and human powered hydraulic pumping.[7,8] The fixed layouts of continuous microfluidics employed in these devices, however, limit their scalability and flexibility, making it difficult to adapt them on the fly to different protocols.

In digital microfluidics (DMF), droplets containing samples or reagents are manipulated to carry out a range of discrete fluidic operations. Precise control of individual droplets can be achieved, thus providing greater flexibility and facilitating the implementation of multi-step reactions.[9,10]

The electrowetting on dielectric (EWOD) phenomenon[11] is one of the most common actuation mechanisms used in DMF and has been widely adopted in biomedical[12-16] and, sometimes, other applications.[17,18] Traditional EWOD devices, however, still require an external high-voltage supply and switching circuitry, which require significant custom development to realize compact systems.[19]

We report EWOD-based DMF with finger-actuated voltage generation on chip, or F-DMF, to eliminate the need for external voltage sources. Fig. 1 schematically illustrates one possible implementation of our device concept, which uses an array of piezoelectric elements to convert mechanical energy pulses provided by human fingers to voltage pulses. Using this scheme, we confirmed basic modes of droplet
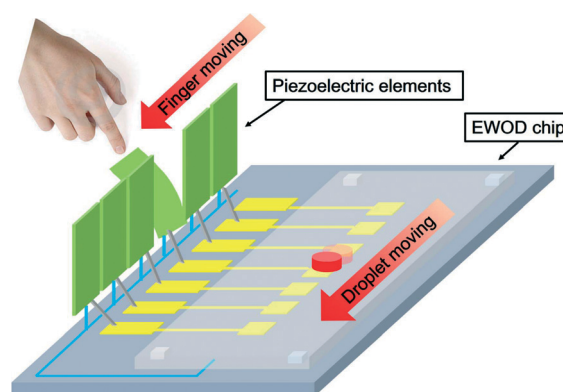

Fig. 1 Schematic of one implementation for the finger-actuated digital microfluidic platform. The piezoelectric elements convert mechanical energy imparted by human fingers to electrical energy to actuate droplets confined between two parallel plates through the electrowetting on dielectric (EWOD) phenomenon.

[a] *Department of Mechanical and Aerospace Engineering, University of California, Los Angeles, CA, USA. E-mail: just@seas.ucla.edu*
[b] *Department of Bioengineering, University of California, Los Angeles, CA, USA*

manipulation, such as transport, splitting and merging of water droplets.[20] Furthermore, to demonstrate its capability for biomedical applications, we successfully performed the key assay steps involved in glucose detection and an immunoassay.

EWOD device

Device design and fabrication

To successfully manipulate micro-droplets using EWOD, one must generate voltage pulses of sufficient amplitude to overcome capillary, inertial, and viscous forces. The EWOD-induced contact angle change is related to the applied voltage by the Lippmann–Young equation:

$$\cos\theta(V) - \cos\theta_0 = \frac{\varepsilon_0 \varepsilon}{2\gamma_{LG} t} V^2 \qquad (1)$$

where θ_0 denotes the equilibrium contact angle at $V = 0$ V, ε_0 is the permittivity of vacuum, ε is the dielectric constant of the dielectric layer separating the droplet from the electrode, t is its thickness, and γ_{LG} is the surface tension between the droplet and surrounding. Since the contact angle change represents the actuation force along the surface, the higher the applied voltage the stronger the actuation force that will drive the droplet against the above-mentioned resistant forces. Because the capillary resistance originated from the contact angle hysteresis of an aqueous droplet surrounded in air (as opposed to the popular oil environment) is larger than the inertial or viscous resistance in most cases, performance of EWOD devices is often measured in the air environment without resorting to the filler oil or oil impregnation.[11] To manipulate water droplets in air, typical EWOD devices require a voltage source of about 40 V.[20]

Our EWOD devices consist of two parallel glass plates that were separated by approximately 100 μm. The bottom glass plate contains an array of 1×1 mm² gold electrodes, which was fabricated using standard micro-fabrication processes. We first deposited a 20 nm Cr/100 nm Au layer on a glass wafer and patterned the layer by wet etching. Then, we deposited a dielectric layer of silicon nitride by PECVD (plasma enhanced chemical vapor deposition). We next spin coated a solution of Teflon® AF (2% wt/wt in Fluorinert FC-40) at 2000 rpm for 30 seconds and baked it at 180 °C for 10 minutes to obtain a ~100 nm-thick hydrophobic topcoat. A shadow mask was used to define electrical contact pads. The top glass plate was coated with a transparent conductive ITO (indium tin oxide, <15 ohm per square) layer to form a counter electrode for EWOD. The counter electrode was also coated with a ~100-nm-thick layer of Teflon®.

Due to the finite energy conversion efficiency of our piezoelectric elements and safety consideration in portable applications, a low threshold actuation voltage and therefore a thin dielectric layer is desired. However, a thin dielectric layer is less robust and prone to pinholes and other defects, which lead to electrolysis-induced failure of EWOD devices. The

dielectric layer thickness is further limited by the capacitance allowed per EWOD electrode, which must be kept below that of the piezoelectric element to minimize the voltage dividing effect. With the above considerations in mind, we examined SiNx layers of thickness ranging from 0.8 μm to 2.5 μm as our dielectric layers. The estimated capacitance is approximately 60 pF per electrode for the EWOD devices with a 0.8 μm-thick dielectric layer, which is much smaller than that of the piezoelectric element (~1 nF).

EWOD actuation voltage

To characterize the threshold actuation voltage required for EWOD actuation as a function of the dielectric layer thickness, an external programmable power source was used to apply precisely defined voltage pulses. A water droplet of ~0.3 μL in volume was spotted onto the EWOD device and subsequently split into two nominally identical daughter droplets. After one of these droplets was positioned on one of the electrodes, the amplitude of the voltage pulse applied to the adjacent electrode was gradually increased until the droplet was successfully transported.

The threshold actuation voltage was recorded for each dielectric layer thickness and the results are plotted in Fig. 2 (symbols). Also shown as a solid line in Fig. 2 are the voltages required theoretically (eqn (1)) for the contact angle to change from 120° to 70°, which is an empirically determined range for droplet actuation in the given EWOD device. In general, the threshold actuation voltage increases with the increasing dielectric layer thickness. For EWOD devices with a PECVD SiNx dielectric layer of thickness approximately 2.5 μm, a voltage as large as 70 V is required for successful actuation of a water droplet.

Mechanical energy conversion

Piezoelectric elements of 13×25 mm² were used to convert a mechanical energy input by human fingers into voltage pulses to actuate micro-droplets in our EWOD DMF devices.
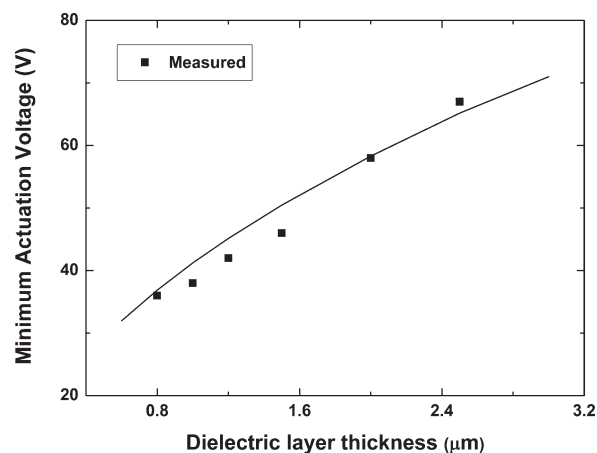
Fig. 2 Threshold actuation voltage of a water droplet on EWOD devices as a function of the thickness of PECVD SiNx dielectric layers.

Each piezoelectric element consists of a PVDF (polyvinylidene fluoride) layer of thickness 28 μm (piezoelectric layer) laminated on a polyester layer of thickness 125 μm (substrate layer) as illustrated in Fig. 3(a) to maximize the average strain in the piezoelectric layer and hence its output voltage. The length of the piezoelectric layer, L_p, is approximately 20.5 mm.

We modelled each piezoelectric element as an Euler–Bernoulli beam. The element (beam) is mounted vertically with the clamped end fixed. The bending angle, $\alpha(s)$, is defined as the rotation of the piezoelectric element beam measured in radians at distance s from the fixed end, as illustrated in Fig. 3(b). For a single piezoelectric element, the open circuit voltage can be expressed as:[21,22]

$$V_0 = \frac{e_{31} h_p}{\varepsilon^s} \overline{S}_1 \tag{2}$$

Here, e_{31} is the electromechanical coupling coefficient of the piezoelectric layer, ε^s is the permittivity of the piezoelectric layer under a constant strain and h_p is the thickness of the piezoelectric layer.

The average strain, $\overline{S}_1$, is defined as:

$$\overline{S}_1 = \frac{\int\limits_{L_p} \int\limits_{h_1}^{h_2} (\frac{\partial \alpha}{\partial s}) y \, dy \, ds}{L_p h_p} = \frac{(\alpha_{tip} - \alpha_0) \int\limits_{h_1}^{h_2} y \, dy}{L_p h_p} \tag{3}$$

where h_1 and h_2 are the distances from the neutral axis of the whole beam to the bottom and top of the piezoelectric layer, respectively; α_{tip} and α_0 are the bending angles, $\alpha(s)$, at the tip and at the starting end of the piezoelectric layer, respectively (Fig. 3(b)).

To characterize the energy conversion capability of our piezoelectric elements, the open-circuit voltage outputs were measured using an electrometer of input impedance >200 TΩ. Optical images of the side views of the element were captured to extract the bending angles along the beam.

Fig. 4 shows the measured and predicted output voltages as a function of the tip bending angle, α_{tip}, for a single piezoelectric element. The prediction (straight line) agrees reasonably well with the experimental results (symbols) over the entire range. Output voltages greater than 40 V, which are

Fig. 4 Open-circuit output voltages of a single piezoelectric element as a function of the tip bending angle.

sufficient to reliably actuate a water droplet in the EWOD device with a ~0.8 μm-thick SiNx dielectric layer, can be generated at tip bending angles greater than 80°. However, larger deformations may not be desirable for field operations and may also lead to degradation of the piezoelectric elements. We estimated that the force required to achieve a bending angle of 36, 70 and 108° is approximately 0.06, 0.12 and 0.18 N, respectively.

If needed, multiple piezoelectric elements may be connected electrically in series and mechanically in parallel to increase the output voltage while limiting required deflection to an acceptable range. Fig. 5 shows the total output voltage of single and two or three piezoelectric elements connected in series. The results are shown for three different bending angles. At relatively small tip bending angles (~15°), the total voltage output increases linearly with each additional piezoelectric element. At larger tip bending angles (45° and 90°), adding more elements does not lead to a proportionate increase in the output voltage. This is in part due to asynchronous bending of each element and in part to finite leakage currents. Nevertheless, we demonstrated that output voltages on
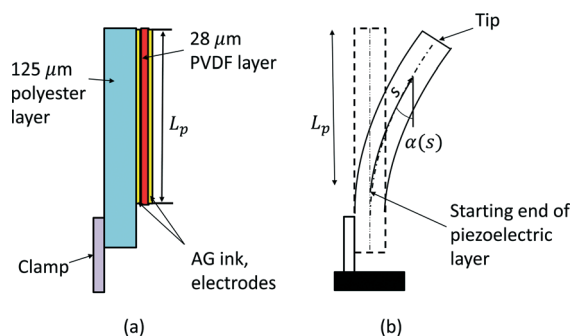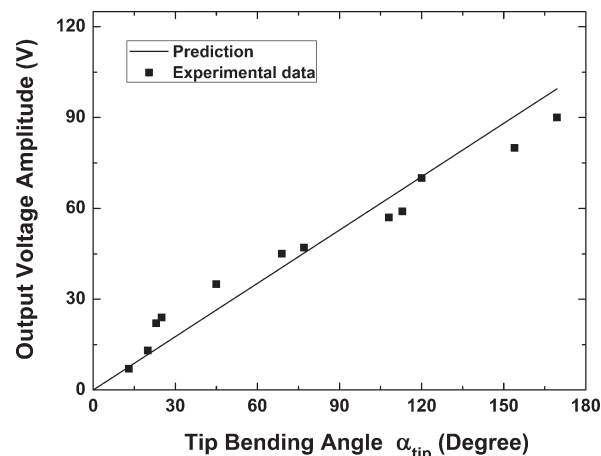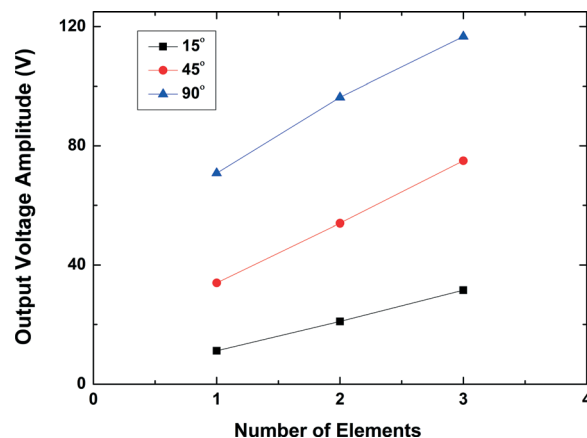

Fig. 3 (a) Cross section of the main functional layers of a laminated piezoelectric element used in the present study; (b) definitions of the length, L_p, and the bending angle, α.

Fig. 5 Total voltage outputs from multiple piezoelectric elements connected in series under different tip bending angles.

the order of 100 V can be reliably generated using piezoelectric elements connected in series with tip bending angles <90°.

EWOD actuation of micro droplets

Basic droplet operations

We next demonstrated successful finger-powered actuation of water droplets on EWOD devices with 0.8 μm-thick PECVD SiNx dielectric layers. An array of single piezoelectric elements is used to convert mechanical energy to voltage pulses. Fig. 6 shows optical images of a single water droplet (~0.15 μL) being transported over adjacent electrodes through a sequence of finger-driven deflection of the piezoelectric elements. To avoid a droplet being trapped on an inactive zone between two adjacent electrodes, we delayed the release of the previously bent piezoelectric element while deflecting the neighbouring element. For example, referring to Fig. 6, element 2 was not entirely released when element 3 was deflected, such that the front contact line of the droplet would stay across the gap between electrodes 2 and 3. For such a delayed release, a holding force of approximately 0.06 N is sufficient.

We also demonstrated droplet splitting by simultaneously deflecting two non-adjacent piezoelectric elements while keeping the middle one non-deflected. Fig. 7 illustrates a splitting of a water droplet (~0.3 μL) into two daughter droplets of similar sizes through simultaneous deflection of element 1 and 3. When splitting was in order, the droplet was
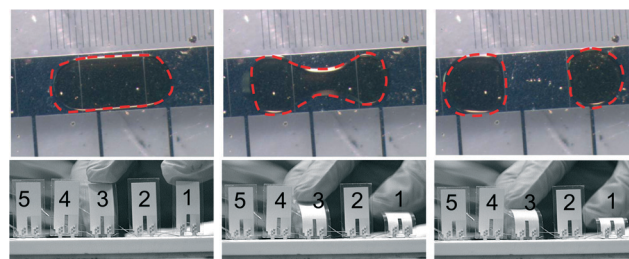
Fig. 7 Finger-actuated EWOD droplet splitting. The piezoelectric elements 1 and 3 are bent simultaneously for splitting.

elongated in the longitudinal direction by a wetting force exerted at the two ends while keeping the middle non-wetting, as shown in Fig. 6. The actuation voltage on either side is approximately 40–50 V, produced by one single piezoelectric element with a bending angle <90°. For a large droplet that covers multiple electrodes, asymmetric splitting can also be achieved by simultaneously deflecting a set of piezoelectric elements connected to the electrodes in an asymmetric manner, for example, elements 1 and 3, 4. Fig. 8 shows a merging of two droplets of similar sizes by asynchronous bending and release of three piezoelectric elements (2, 4, and 3).

Applications to biological assays

As proof of principle demonstration of biological applications of our F-DMF, we performed basic steps of glucose detection and immunoassay. In these experiments, where higher EWOD voltages are necessary to actuate droplets, we used silicon nitride layers of thickness 2.5 μm because they help prevent electrolysis of water under our low-frequency (~1 Hz) finger-driven actuation scheme. Two piezoelectric elements connected in series were used to provide an actuation voltage of up to 100 V.

We demonstrated glucose detection based on an enzymatic oxidation, where the color of an assay solution changes from clear to brown in the presence of glucose. Since the reagent solution may chemically attack the hydrophobic coatings, we pre-treated both the upper plate and bottom substrate of our EWOD devices with silicone oil. A reagent solution was prepared by adding 0.8 mL of *o*-dianisidine reagent to an amber bottle containing 39.2 mL of a 1:5 horseradish peroxidase/glucose oxidase solution (15 units of protein per mL of solution). We spotted a droplet of a 1 mg mL^{-1}
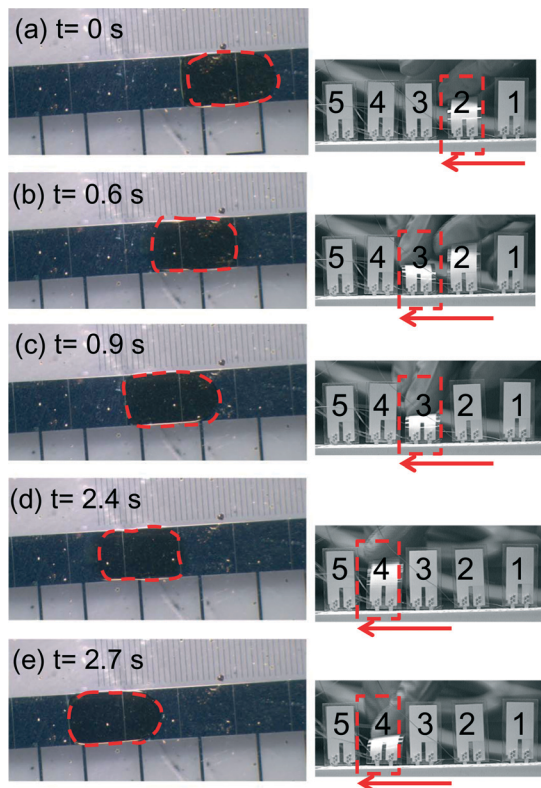

Fig. 6 Finger-actuated EWOD transport of a water droplet where actuation voltage pulses were provided by bending a series of piezoelectric elements.
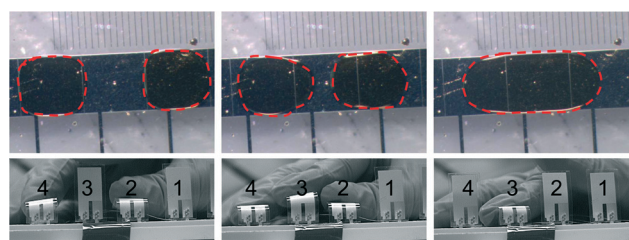

Fig. 8 Finger-actuated EWOD droplet merging.

standard glucose solution and another one of a reagent solution (both of approximately 0.15 μL) onto the bottom plate and covered with the top plate. The reagent droplet was then transported towards the glucose sample droplet and merged, as shown in Fig. 9(b–d). An optical image was taken to verify the color change indicative of successful enzymatic oxidation reaction. We observed that the brown color started developing after the merging and fully developed after a 5 minute incubation, as shown in Fig. 9(e).

We next performed an immunoassay-related enzyme-based colorimetric reaction using the F-DMF. 5-Bromo-4-chloro-3-indolyl blue tetrazolium (BCIP/NBT) is a commonly used substrate for alkaline phosphate (ALP). In our experiment, the enzyme substrate was used to detect an ALP conjugated antibody. This mimicked the last step of signal detection and amplification in ALP-based colorimetric ELISA.[23] To prepare the experiment, an ALP conjugated IgG antibody (2.5 mg mL^{-1}) was first diluted to approximately 13 μg mL^{-1}. The antibody was immobilized on the upper plate of our EWOD device by manual pipetting of ~500 nL of the diluted solution. The upper plate was chosen due to the smaller interference with actuation compared with the bottom plate. Spots were allowed to air-dry before use. Approximately 0.15 microliter aliquots of the enzyme substrate (BCIP/NBT) solution (BCIP: 0.15 mg mL^{-1}, NBT: 0.3 mg mL^{-1}, Tris buffer: 100 mM, and MgCl$_2$: 5 mM) was loaded onto the bottom plate of the EWOD device, as shown in Fig. 10(a). Voltage pulses provided by finger-driven actuation were then used to move the sample droplet towards the immobilized antibody spot, as illustrated in Fig. 10(b–c). After ~5 minute incubation, black-purple precipitates were confirmed to be produced (Fig. 10d), indicating the detection of the ALP-conjugated antibody.

Conclusions

In summary, we demonstrated finger-actuated digital microfluidics based on the electrowetting-on-dielectric (EWOD)
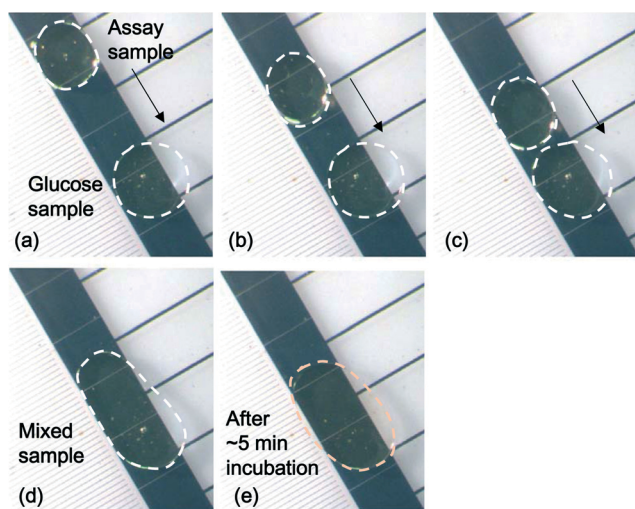

Fig. 9 Snapshots of sample and reagent droplet during a glucose assay and enzyme catalyzed formation of colored product.
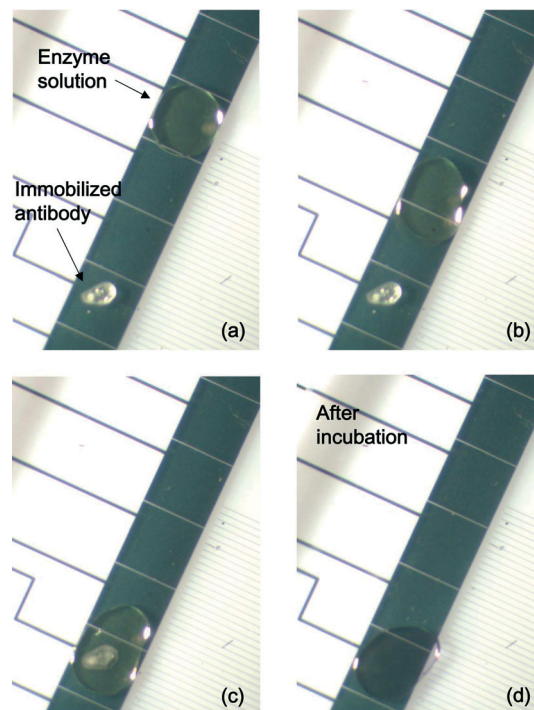

Fig. 10 (a)–(c) Frames from a video depicting a droplet of the BCIP/NBT enzyme solution transported towards an immobilized antibody spot upon finger actuation and (d) purple precipitation observed indicating detection of an ALP conjugated antibody.

phenomenon by using piezoelectric energy conversion of human power. We demonstrated generation of voltage pulses of amplitudes >100 V using laminated polymer piezoelectric elements connected in series. Using the scheme, we confirmed basic EWOD droplet operations such as droplet transport, splitting and merging and further demonstrated an implementation of basic assay steps in glucose detection and immunoassay. Due to the low-frequency nature of finger actuation, a relatively thick dielectric layer was used to help prevent possible electrolysis. Our work offers a promising solution for expanded applications of EWOD-based digital microfluidics in portable systems.

Acknowledgements

References

1 L. Gervais, N. de Rooij and E. Delamarche, *Adv. Mater.*, 2011, **23**, H151–H176.

2 K. A. Addae-Mensah, Y. K. Cheung, V. Fekete, M. S. Rendely and S. K. Sia, *Lab Chip*, 2010, **10**, 1618–1622.

3 A. K. Yetisen, M. S. Akram and C. R. Lowe, *Lab Chip*, 2013, **13**, 2210–2251.

4 A. W. Martinez, S. T. Phillips, G. M. Whitesides and E. Carrilho, *Anal. Chem.*, 2010, **82**, 3–10.

5   Y.-C. Su, L. Lin and A. P. Pisano, *J. Microelectromech. Syst.*, 2002, **11**, 736–742.

6   I. K. Dimov, L. Basabe-Desmonts, J. L. Garcia-Cordero, B. M. Ross, A. J. Ricco and L. P. Lee, *Lab Chip*, 2011, **11**, 845–850.

7   K. Iwai, R. D. Sochol, L. P. Lee and L. Lin, *Proc. MEMS*, 2012, 949–952.

8   W. Li, T. Chen, Z. Chen, P. Fei, Z. Yu, Y. Pang and Y. Huang, *Lab Chip*, 2012, **12**, 1587–1590.

9   M. J. Jebrail, M. S. Bartsch and K. D. Patel, *Lab Chip*, 2012, **12**, 2452–2463.

10   R. Sista, Z. Hua, P. Thwar, A. Sudarsan, V. Srinivasan, A. Eckhardt, M. Pollack and V. Pamula, *Lab Chip*, 2008, **8**, 2091–2104.

11   W. C. Nelson and C.-J. Kim, *J. Adhes. Sci. Technol.*, 2012, **26**, 1747–1771.

12   P. Y. Keng, S. Chen, H. Ding, S. Sadeghi, G. J. Shah, A. Dooraghi, M. E. Phelps, N. Satyamurthy, A. F. Chatziioannou, C.-J. Kim and R. M. van Dam, *Proc. Natl. Acad. Sci. U. S. A.*, 2012, **109**, 690–695.

13   H. Moon, A. R. Wheeler, R. L. Garrell, J. A. Loo and C.-J. Kim, *Lab Chip*, 2006, **6**, 1213.

14   E. M. Miller, A. H. C. Ng, U. Uddayasankar and A. R. Wheeler, *Anal. Bioanal. Chem.*, 2011, **399**, 337–345.

15   V. Srinivasan, V. K. Pamula and R. B. Fair, *Lab Chip*, 2004, **4**, 310–315.

16   A. H. C. Ng, K. Choi, R. P. Luoma, J. M. Robinson and A. R. Wheeler, *Anal. Chem.*, 2012, **84**, 8805–8812.

17   P. Sen and C.-J. Kim, *J. Microelectromech. Syst.*, 2009, **18**, 174–185.

18   W. C. Nelson, H. P. Kavehpour and C.-J. Kim, *Lab Chip*, 2011, **11**, 2424–2431.

19   J. Gong, S.-K. Fan and C.-J. Kim, *Proc. Int. Conf. MEMS*, 2004, 355–358.

20   S. K. Cho, H. Moon and C.-J. Kim, *J. Microelectromech. Syst.*, 2003, **12**, 70–80.

21   Q.-M. Wang, X. Du, B. Xu and L. E. Cross, *J. Appl. Phys.*, 1999, **85**, 1702.

22   N. G. Elvin and A. A. Elvin, *J. Intell. Mater. Syst. Struct.*, 2012, **23**, 1475–1484.

23   H. Chen, J. Cogswell, C. Anagnostopoulos and M. Faghri, *Lab Chip*, 2012, **12**, 2909–2913.